Adsorption Properties of MgO(111) Nanoplates for the Dye Pollutants from Wastewater

Juncheng Hu,*,† Zhi Song,† Lifang Chen,‡ Haijian Yang,† Jinlin Li,† and Ryan Richards*,§

Key Laboratory of Catalysis and Materials Science of the State Ethnic Affairs Commission and Ministry of Education, South-Central University for Nationalities, Wuhan, 430074, P.R. China, State Key Laboratory of Chemical Engineering, East China University of Science and Technology, Shanghai, 20023, P.R. China, and Department of Chemistry and Geochemistry, Colorado School of Mines, Golden, Colorado, 80401

Nanoplates of MgO possessing the polar (111) facet as the primary surface were studied as adsorbents for dye pollutants removal from wastewater. The thickness of the MgO(111) nanoplates is (3 to 5) nm, with an average specific surface area (SSA) of 198 $m^2 \cdot g^{-1}$. Congo red and reactive brilliant red X3B are used as model azo dyes, and their adsorption is studied at different dye concentrations, solution pH, salt concentration, and temperatures in a batch reactor. The experimental results indicate that the MgO nanoplates with polar (111) surfaces exhibited much more favorable adsorption properties than a conventionally decomposition prepared MgO powder (CP-MgO, SSA = 30 $m^2 \cdot g^{-1}$) and activated carbon (SSA = 1500 $m^2 \cdot g^{-1}$) for Congo red solution with the initial concentration of 100 $mg \cdot L^{-1}$ in 30 min. The maximum adsorption capability of Congo red on MgO (111) nanosheets reached 131.3 $mg \cdot g^{-1}$ in 30 min, while the maximum adsorption capabilities of Congo red on CP-MgO and activated carbon were only (61.9 and 17.7) $mg \cdot g^{-1}$, respectively. Two common models, the Langmuir and Freundlich isotherms, are used to explicate the interaction of dye and MgO(111). The isotherm evaluations revealed that the Langmuir model attained better fits to the experimental equilibrium data than the Freundlich model. The maximum predicted adsorption capacities were (303.0 and 277.8) $mg \cdot g^{-1}$ for Congo red and reactive brilliant red X3B, respectively. In addition, adsorption kinetic data followed a pseudosecond-order rate for both dyes. Furthermore, compared to activated carbon, the adsorbent MgO(111) has the advantage in that it can be readily regenerated by a simple calcination process and reused without loss of activity. Therefore, it may be well suited for dealing with the removal of dyes from wastewaters.

Introduction

The textile industry is an important component of the modern economy and especially so in Asia. According to a recent study, approximately 700 000 tons of different dyes are produced annually in the world, and more than 60 % of the world dye production is consumed by textile industries.[1] The waste effluent from the textile industry can be particularly problematic due to the presence of hazardous wastes and toxic pollutants in the final effluent. Among them, organic dyes are one of the major groups of pollutants in wastewaters. In China, over $1.6 \cdot 10^9$ m^3 of dye-containing wastewater per year is drained into environmental water systems without having been properly treated. The release of toxic and hazardous dyes from the textile industry has created a global concern due to their considerable toxicity. Dyes impart undesirable color to water and are often lethal for aquatic life. Furthermore, one of the most marked features of modern dyes is their high degree of chemical, photolytic, and microbiological stability. Thus, dyes are not readily degradable under aerobic conditions prevailing in conventional biological treatment processes.[2,3] The elimination of all pollutants is the current wastewater treatment goal, and various treatment methods have been developed for decontamination purposes including coagulation, chemical oxidation, membrane separation, electrochemical processes, and adsorption techniques. Physical adsorption is generally considered to be an effective method for quickly lowering the concentration of dissolved dyes in an effluent.[4] A considerable amount of the literature also reports the adsorption of dyes on various adsorbent surfaces such as activated carbon,[5,6] silica,[7] clay,[8,9] natural polymers,[10,11] synthetic polymers,[12,13] waste materials,[14,15] various nanotubes,[16,17] glass fiber,[18] alumina,[19] and so forth. In recent years, novel MnO_2 and Fe_2O_3 nanostructures have been found to effectively remove pollutants from wastewater.[20,21] The pollutant adsorbs onto the solid adsorbent surface from the effluent, and the quantity of pollutant removed depends on the adsorption capacity of the adsorbent. It would be desirable to recycle the adsorbents to avoid disposing of the adsorbate/adsorbent system. Over the years, a variety of techniques have been developed for the regeneration of activated carbon. These methods are based either on desorption, induced by displacement with a solvent, or on decomposition induced by thermal,[22] chemical,[23] electrochemical,[24] or microbial processes.[25] These methods have some disadvantages including high temperature, high pressure, or the production of secondary pollution and have hindered the development of activated carbon regeneration and reuse. Metal oxides have potential applications in water treatment because of their high surface area in addition to low production and regeneration costs. Therefore, it is desirable to obtain efficient and recyclable metal oxide adsorbents.

* To whom correspondence should be addressed. E-mail: junchenghuhu@hotmail.com; rrichard@mines.edu.
† South-Central University for Nationalities.
‡ East China University of Science and Technology.
§ Colorado School of Mines.

10.1021/je100274e
Published on Web 07/16/2010

Recently, much attention has been paid to nanotechnology, and several papers have reported the application of various nanoparticles for the treatment and remediation of pollutants in the environment,[26−28] some even focusing specifically on dye removal.[29,30] Nanoscale materials have high surface areas and a large fraction of atoms available for chemical reaction. Nanoscale alkaline earth metal oxides, in particular MgO, are very promising materials for applications as adsorbents due to their destructive sorbent properties,[31] high surface reactivity and adsorption capacity compared to their commercial analogues,[32] and the simplicity of their production from abundant natural minerals. Furthermore, as the pH of the zero point of charge (pH_{zpc}) of MgO is 12.4,[33] it is a suitable adsorbent for adsorption of anions due to its favorable electrostatic attraction mechanism. In recent years, MgO nanoparticles have been found to have a good ability to remove azo and antroquinon reactive dyes from wastewater.[34] The traditional method for the preparation of MgO is the thermal decomposition of either magnesium salts or magnesium hydroxides, which results in the inhomogeneity of morphology and crystallite size. Much effort has been exerted to prepare MgO possessing controlled shapes and morphologies implying the importance of controlling size and shape in MgO synthesis.[35−37] Recently, we have developed a simple method to prepare sheet-like MgO and NiO with the highly ionic (111) facet as the major surface of the nanoplates and found that NiO(111) nanosheets were good adsorbents for organic dyes.[38−41]

In the present study, Congo red and reactive brilliant red X-3B were used as typical dye pollutants, and MgO(111) nanoplates as an absorbent for the removal of these dye pollutants from aqueous solution were investigated. For comparison, the removal capacity of Congo red on conventionally prepared MgO powder (CP-MgO) obtained from magnesium nitrate thermal decomposition and activated carbon were studied. The MgO(111) nanosheets showed a much better ability to remove Congo red than CP-MgO powder and activated carbon. The effects of various experimental parameters, including pH of the solution, exposure time, temperature, and ionic strength, were investigated. Adsorption isotherms and kinetics were also analyzed.

Experimental Section

Materials. Reactive brilliant red X-3B and Congo red were purchased from the Tianjin Chemicals Company; they were not purified prior to use. Dye solutions were prepared by dissolving these dyes in distilled water. The activated carbon with a surface area of 1500 $m^2 \cdot g^{-1}$ was also purchased from the Tianjin Chemical Company.

Preparation of MgO(111) Nanoplates and Conventionally Prepared MgO Powder. MgO(111) nanoplates were prepared using "green" procedures that have been reported by ourselves recently, using Mg ribbon as a starting material.[38] Here, we prepared the MgO(111) nanoplates in the absence of urea. Thus, in a typical synthesis of the MgO nanoplates, 1.0 g (42 mmol) of Mg ribbon was cleaned with sandpaper and acetone, and then the ribbon was cut into small pieces and reacted with absolute methanol under a static argon atmosphere. After the Mg ribbon was completely dissolved, 4-methoxyl-benzyl alcohol (BZ) was added to the mixture in the ratio Mg/BZ = 2 (molar ratio); after stirring for 5 h, H_2O (molar ratio of 2 with respect to Mg) was dissolved into 30.0 mL of methanol and was added dropwise into the system under stirring, and the mixture was stirred for 12 h before being transferred to a 600 mL Parr autoclave (P_{max} = 200 bar, T_{max} = 350 °C). The autoclave containing the reaction mixture was purged with Ar for 10 min, and then a pressure of 10 bar of Ar was imposed before initiation of heating. The mixture was heated to 265 °C and maintained for 15 h continuously, and then, the vapor inside was vented (thereby removing the solvent in the supercritical state). A dry white powder was collected and calcined with a ramp rate of 3 °C·min^{-1} to 500 °C and then maintained at 500 °C for 6 h. The ultrafine white powder produced from the above contains solely the MgO nanoplates.

Conventionally prepared MgO (CP-MgO) was prepared by decomposition of magnesium nitrate at 500 °C for 6 h and possessed a surface area of 30 $m^2 \cdot g^{-1}$.

Characterization. Transmission electron microscopy and electron diffraction characterization of the samples were carried out on a FEI Tecnai F20 S-Twin operated at 200 kV. The samples were prepared by spreading an ultrasonicated suspension in ethanol onto a grid and evaporating the solvent. N_2 adsorption−desorption isotherms were obtained using a Micrometrics ASAP 2020. The samples were degassed at 300 °C in vacuum for more than 4 h prior to the measurement. The specific surface areas (SSAs) were evaluated with the Brunauer−Emmett−Teller (BET) method in the P/P_0 range of 0.05 to 0.35.

Adsorption Experiment. Dye adsorption on the MgO(111) nanoplates was performed in a batch system at room temperature. The experiments were conducted individually for each of the model dyes, but the same procedure was used for both, as detailed below. MgO(111) nanoplates (0.015 g) were added into 20 mL of a dye pollutant solution with various concentrations [(50 to 400) mg·L^{-1}] under stirring at a rate of 150 rpm. At the end of the adsorption period, the solution was centrifuged for 5 min at 7000 rpm. After centrifugation, small amounts of the liquid were taken to be analyzed by UV−vis (UV-2550, Shimadzu, Japan) absorption spectroscopy by monitoring the absorbance changes at a wavelength of maximum absorbance after being diluted 5 times. The dye removal efficiency was determined using the follow expression:

$$\text{Dye removal efficiency (\%)} = \frac{(C_0 - C_f)}{C_0} \cdot 100$$

where C_0 and C_f represent the initial and final (after adsorption) dye concentrations, respectively. The investigated ranges of the two dye concentrations were as follows: Congo red concentration [(100 to 400) mg·L^{-1}] and X3B concentration [(50 to 300) mg·L^{-1}]. For comparison, the same experiments were performed on CP-MgO and activated carbon. A 0.015 g amount of the adsorbent was added into 20 mL of a Congo red pollutant solution with an initial dye concentration of 100 mg·L^{-1}. The Mg ion concentration was analyzed by atomic absorption spectroscopy using an AA-6300 apparatus from Shimadzu.

To study the interaction between dye and MgO(111), the experiments were performed under different experimental conditions. The effects of the medium pH on the adsorption capacities of the MgO(111) nanoplates were investigated in the pH range of 3.0 to 12.0. The pH was adjusted with 0.1 M HCl and 0.1 M NaOH solutions, and the pH of each solution was measured by using a laboratory scale pH meter (PHS-25). The effects of the temperature on the adsorption capacities of the MgO(111) nanoplates were investigated at (283, 313, and 333) K. In addition, different concentrations of NaCl [(0, 0.25 and 0.5) M] were investigated to evaluate the salt effects on the adsorption capacities of the MgO(111) nanoplates.

Results and Discussion

Characterization of MgO(111) Nanoplates. The MgO nanoplates possessing the (111) plane as the main surface have been

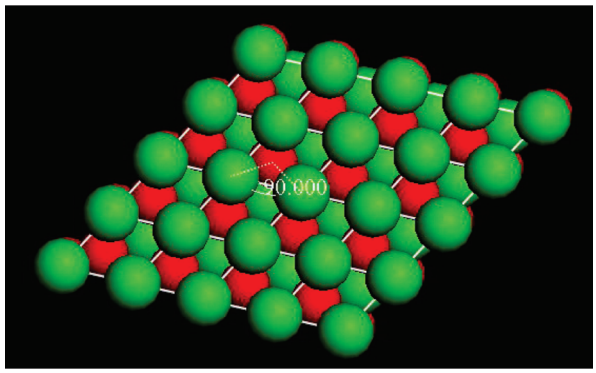

Figure 1. Illustration of the (111) facet of MgO.

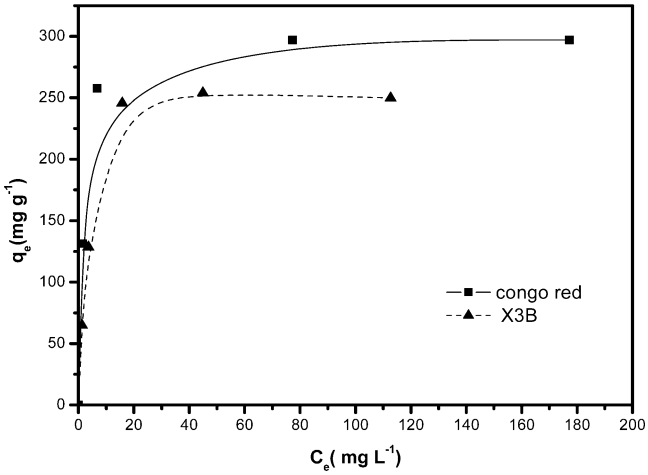

Figure 2. Effect of initial dye concentration on the removal of dye on MgO(111). (Initial dye concentration: Congo red (100 to 400) mg·L^{-1}, X3B (50 to 300) mg·L^{-1}; temperature: 283 K; MgO(111) dosage: 0.75 g·L^{-1}.)

characterized by a combination of bright-field transmission electron microscopy (BF-TEM) and high-resolution transmission electron microscopy (HRTEM) as well as X-ray and electron diffraction. BF-TEM of the calcined MgO samples reveals that the material crystallizes, forming nanoplates with a typical diameter of (50 to 200) nm and a thickness of typically (3 to 5) nm (Figures S1 and S2, Supporting Information).[38] HRTEM analysis of isolated MgO nanoplates shows that the main surface of the nanoplates is the (111) lattice planes. The MgO(111) facet is composed of exclusively oxygen on one layer and exclusively magnesium atoms on the other layer (Figure 1); thus, positive or negative, the surface of MgO(111) has a strong electropolarity. The MgO(111) nanoplates have a surface area of 198 m^2·g^{-1}.

Effect of Dye Concentration. The effect of initial dye concentration on the adsorption capacity of the MgO(111) nanoplates was investigated under equilibrium conditions with a concentration of 0.75 g·L^{-1} of adsorbent. In Figure 2, a similar dye adsorption profile was observed, where the adsorption capacity increased with an increase in the dye concentration. The maximum adsorption capabilities of the two dyes on MgO(111) nanoplates reached (254.3 and 297.0) mg·g^{-1} for reactive brilliant red X-3B and Congo red, respectively. We propose that an increase in the initial dye concentration leads to an increase in the mass gradient between the solution and the adsorbent and thus acts as a driving force for the transfer of dye molecules from solution to the particle surface. The increase in the proportional dye adsorption is attributed to an equilibrium shift during the MgO(111) adsorption process.

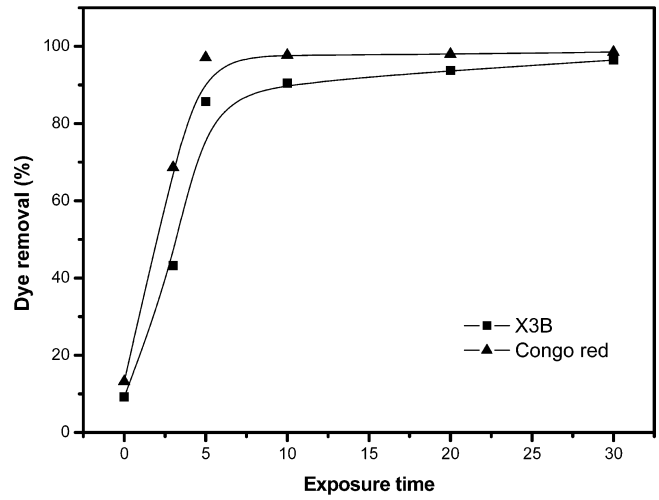

Figure 3. Effect of stirring time on the removal of Congo red and X3B. (MgO(111) dosage: 0.75 g·L^{-1}; initial dye concentration: 100 mg·L^{-1}; temperature: 283 K.)

Effect of Exposure Time. The exposure time between adsorbate and adsorbent is one of the most important parameters that affects the performance of adsorption processes. The effect of exposure time on the performance of MgO(111) nanoplates in adsorbing Congo red and X3B was investigated individually. The initial dye concentration for all solutions was 100 mg·L^{-1}. Figure 3 shows removal efficiencies for the two dyes as a function of exposure times ranging between (5 and 30) min. These data indicate that adsorption started immediately upon adding the MgO powder to both solutions. The removal efficiency of Congo red rapidly reached 97.7 % at 10 min. For X3B, the percentage of removal was 9.2 % at 1 min and 93.0 % at 10 min. Therefore, the optimum exposure time of these two dyes on MgO(111) nanoplates was considered to be 10 min under these conditions, potentially lowering operational costs for applications. The contact time obtained for equilibrium adsorption onto MgO(111) is shorter than most of the reported values for dye adsorption onto biomass fly ash, activated carbon, and sawdust.[39−42]

Comparison of Adsorbents. For a sustainable future, environmental problems including water treatment must be addressed with effective new technologies. Activated carbons are widely used to remove organic pollutants from water because of their relatively low cost, inert nature, and high surface area. Thus, for comparison, the adsorption capability of activated carbon and CP-MgO were investigated in this study. In Figure 4, we can see that the removal efficiency of Congo red on MgO(111) nanoplates reached a maximum in 30 min. This investigation further indicated that the MgO(111) nanoplates demonstrated higher adsorption capacity than activated carbon and CP-MgO in a short time. The maximum adsorption capability of Congo red on MgO(111) nanoplates reached 131.3 mg·g^{-1} in 30 min, while the maximum adsorption capabilities of Congo red on CP-MgO and active carbon were only (61.9 and 17.7) mg·g^{-1}, respectively. Furthermore, the Congo red containing MgO(111) nanoplates could be regenerated by combustion at 500 °C in air for 3 h, and the regenerated MgO(111) nanoplates kept almost the same adsorption performance as shown by the dashed line in Figure 4. The Mg ion concentration was analyzed after adsorption to test for magnesium leaching by atomic absorption spectroscopy. There is a trace amount of magnesium in the solution; the concentration was 1.2·10^{-2} mg·mL^{-1}, and 1.6 % of the Mg is leached.

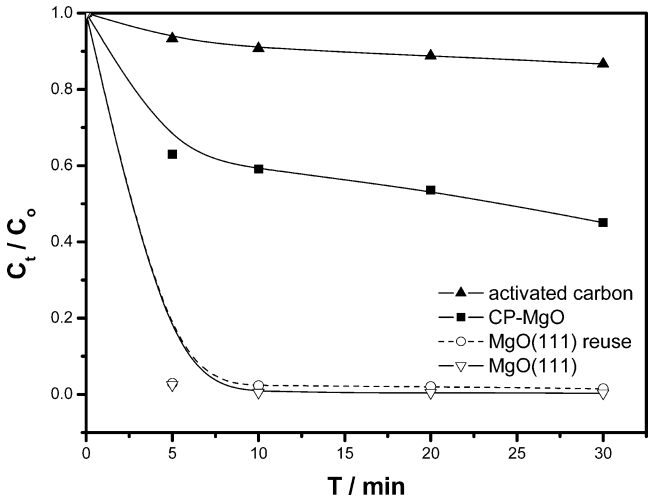

Figure 4. Comparison of various adsorbents on the removal of Congo red. (Adsorbent dosage: 0.75 g·L^{-1}, initial dye concentration: 100 mg·L^{-1}, initial pH: 7.15, stirring time: 30 min.)

An analysis of the adsorption isotherm is of fundamental importance to describe how adsorbate molecules interact with the adsorbent surface. The relationship between equilibrium data and either theoretical or practical equations is essential for interpretation and prediction of the extent of adsorption. Several isotherm models have been developed for evaluating the equilibrium adsorption of compounds from solutions such as Langmuir, Freundlich, Redlich−Peterson, Dubinin−Radushkevich, Sips, Temkin, and so forth. Two of the most commonly applied isotherm theories, Freudlich and Langmuir equilibrium isotherm theories, have been adopted to analyze the data for wastewater treatment applications.

The Freundlich isotherm was employed to describe heterogeneous systems and reversible adsorption, which is not restricted to monolayer formations. The Freundlich model[43] takes the form:

$$q_e = K_F C_e^{1/n} \tag{1}$$

Equation 1 can be rearranged to obtain a linear form by taking logarithms:

$$\log q_e = \log K_F + \frac{1}{n}\log C_e \tag{2}$$

where q_e is the amount of dye adsorbed per unit of adsorbent at equilibrium (mg·g^{-1}), C_e is the concentration of dye solution at equilibrium (mg·L^{-1}), and K_F and n are the Freundlich adsorption isotherm constants. K_F is indicative of the adsorption capacity of the adsorbent, that is, the greater K_F value, the greater adsorption capacity. The other Freundlich constant n is a measure of the deviation from linearity of the adsorption and is used to verify types of adsorption. It is suggested that if n is equal to unity, the adsorption is linear. Furthermore, n below unity indicates that adsorption is a chemical process, whereas n above unity is associated with a favorable adsorption and a physical process.[44] K_F and $1/n$ values can be calculated from the intercept and slope of the linear plot between log C_e and log q_e.

The Langmuir isotherm is based on the assumption that a structure of adsorbent is homogeneous, where all sorption sites are identical and energetically equivalent. That is to say, the adsorption process of each dye molecule onto the surface of MgO(111) should have equal sorption activation energy and demonstrates the formation of monolayer coverage of dye molecule on the surface of MgO(111).

The Langmuir model[45] takes the form:

$$q_e = \frac{Q_e b C_e}{1 + bC_e} \tag{3}$$

For the Langmuir model (eq 3), the constant b (1 mg^{-1}) is related to the energy of adsorption; C_e (mg·L^{-1}), the equilibrium concentration of the dyes in solution; q_e (mg·g^{-1}), the amount of adsorbed dye on the adsorbent surface at equilibrium, and the constant Q_m (mg·g^{-1}) represents the maximum binding at the complete saturation of adsorbent binding sites.

The equilibrium adsorption data of Congo red and X3B onto MgO(111) adsorbent was analyzed using both the Langmuir and the Freundlich models. Model fits to these equilibrium adsorption results of both dyes were assessed based on the values of the coefficient of determination (R^2) of the linear regression plot. The obtained experimental data were fitted with these two models, the plots are shown in Figure 5 and Supporting Information (SI). Table S1 of the SI summarizes the model constants and the coefficients of determination. As shown in Table S1 of the SI, the R^2 of the Langmuir isotherm was greater than that of the Freundlich isotherm for the adsorption of both dyes. This indicates that the adsorption of Congo red and X3B on MgO(111) are better described by the Langmuir model than the Freundlich, suggesting that adsorption occurs as a dye monolayer adsorbed onto the homogeneous adsorbent surface. Table S1 shows that the maximum predicted adsorption capacities were (303.0 and 277.8) mg·g^{-1} for Congo red and reactive brilliant red X3B, respectively. The dye adsorption process is affected by the properties of both dyes and adsorbent. Owing to the similarity of the adsorbent used in all experiments carried out during this study, the difference in adsorption removal and capacity of Congo red and X3B may be attributed to an electrostatic attraction between the polar MgO(111) surface and the dye in solution. The (111) surface consists of alternating polar monolayers of oxygen anions and magnesium cations, and thus, a strong electrostatic field perpendicular to the (111) surface is created.

The closeness of fit for the models used to predict the adsorption of dye was further confirmed by the average relative error (ARE) factor between the experimental data and model estimates of adsorption capacities. ARE can be determined by the following expression

$$\mathrm{ARE}\ (\%) = \frac{100}{n}\sum_{i}^{n}\left|\frac{q_{i,\mathrm{est}} - q_{i,\mathrm{exp}}}{q_{i,\mathrm{exp}}}\right| \tag{4}$$

where $q_{i,\mathrm{exp}}$ and $q_{i,\mathrm{est}}$ are the experimental and estimated adsorption capacities, respectively, and n represents the number of the tests. The values of ARE for the Langmuir and Freundich models are given in Table S1 of the SI. As shown, for Congo red and X3B, the values of ARE in Langmuir are lower than that of Freundlich model, indicating that they fit the Langmuir model better.

Adsorption kinetic models were applied to interpret the experimental data to determine the controlling mechanism of dye adsorption from aqueous solution. The pseudofirst and pseudosecond order reaction rate equations are the most commonly applied models.[46] The pseudofirst order equation or Lagergren's kinetics

equation[47] is widely used for the adsorption of an adsorbate from an aqueous solution. This kinetic method is based on the assumption that the rate of change of solute uptake with time is directly proportional to the difference in saturation concentration and the amount of solid uptake with time.

$$\frac{dq_t}{d_t} = k_1(q_e - q_t) \tag{5}$$

When $q_t = 0$ at $t = 0$, eq 5 can be integrated into the following equation:

$$\ln(q_e - q_t) = \ln q_e - k_1 t \tag{6}$$

where q_t is the amount of dye adsorbed per unit of adsorbent ($mg \cdot g^{-1}$) at time t, k_1 is the pseudofirst order rate constant (min^{-1}), and t is the contact time (min). The adsorption rate constant (k_1) was calculated from the plot of $\ln(q_e - q_t)$ against t.

Ho and McKay[48] presented the pseudosecond order kinetic model as:

$$\frac{dq_t}{d_t} = k_2(q_e - q_t)^2 \tag{7}$$

Integrating eq 7 and noting that $q_t = 0$ at $t = 0$, the obtained equation can be rearranged into a linear form:

$$\frac{t}{q_t} = \frac{1}{k_2 q_e^{\,2}} + \frac{t}{q_e} \tag{8}$$

where k_2 is the pseudosecond order rate constant. The initial adsorption rate, h, at $t \rightarrow 0$ is defined as:

$$h = k_2 q_e^{\,2} \tag{9}$$

The h, q_e and k_2 values can be obtained by a linear plot of t/q_t versus t.

Plots of experimental results of the two model dyes fitted to the selected adsorption models are shown in Figure 6 and the SI. Table S2 of the SI gives a summary of the models and constants along with the coefficients of determination for the linear regression plots of both dyes. As shown in Table S2,

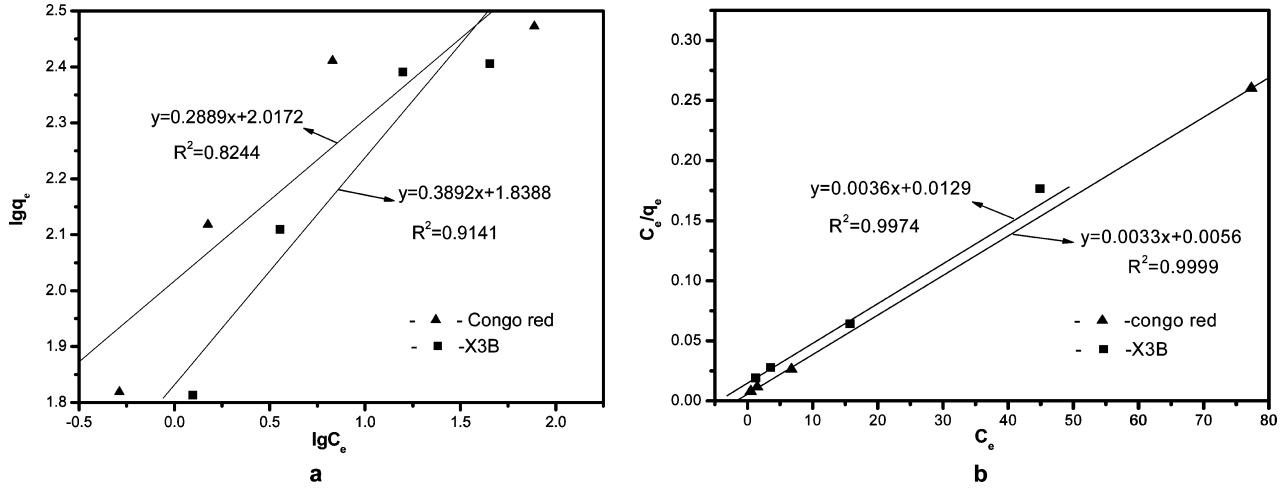

Figure 5. Adsorption isotherm for the adsorption of Congo red and X3B onto MgO (111) nanosheets: (a) Freundlich model, (b) Langmuir model.

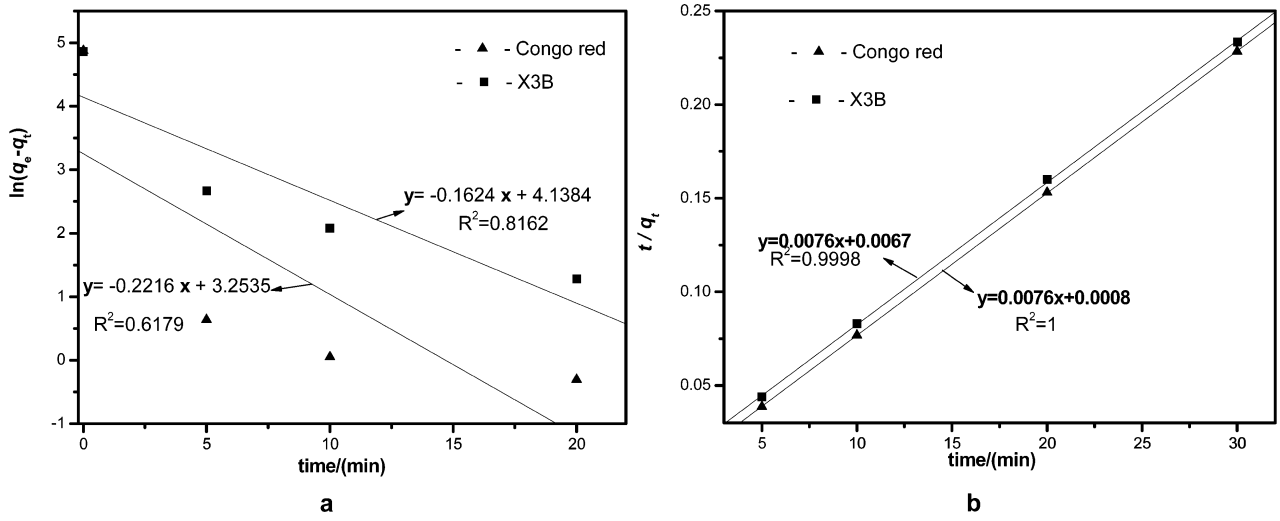

Figure 6. Plots of first and second-order rates for the adsorption of Congo red and X3B onto MgO(111) nanosheets: (a) pseudofirst order rate, (b) pseudosecond order rate.

higher values of R^2 were obtained for the pseudosecond order than for pseudofirst order adsorption rate models, indicating that the adsorption rates of Congo red and X3B onto the MgO(111) nanoplates can be more appropriately described using the pseudosecond order rate rather than pseudofirst order rate. The best fit to the pseudosecond order kinetics indicates that the adsorption mechanism depends on the adsorbate and adsorbent, and the rate-limiting step may be chemisorption involving valence forces through sharing or exchange of electrons. Similar kinetic results have also been reported for the Congo red adsorption onto calcium-rich fly ash,[49] xerogel,[50] and coir pith carbon.[51]

Effect of pH. Solution pH is another important parameter that affects both aqueous chemistry and surface binding sites of the adsorbents. The effect of the initial pH of the solution on the Congo red and X3B adsorption onto MgO(111) nanoplates powder was assessed at different values, ranging from 2 to 13, with a stirring time of 30 min. The initial concentrations of each dye and adsorbent dosage were set at 100 $mg \cdot L^{-1}$ and 0.015 g, respectively, for all batch tests in this experiment. Figure S3 of the SI presents the results of the effect of solution pH on the Congo red and X3B removal efficiencies. As shown in Figure S1, X3B removal increased from (71.0 to 96.4) % when the pH was increased from 2.5 to 5.1. Since the X3B removal increased to its maximum value at a pH of 5.1, the electrostatic attraction between the dye molecules (negatively charged) and the MgO (111) surface (positively charged; pH_{zpc} = 12.4) might be the predominant adsorption mechanism.[52] If this is true, the increase in the pH would result in increasing adsorption capacity. However, X3B removal decreased with increasing pH from 5.1 to 13. The reduction of X3B removal percentage at higher pH might be due to the formation of OH^- and subsequent competition with the X3B molecules for adsorption sites[53] on the surface of MgO(111), leading to the reduction of X3B removal efficiency. As shown in Figure S3, the removal of Congo red was almost independent of pH and remained higher than 97.0 % over the entire range of the experimental pH. Hence, no significant effect of pH was observed on the removal of Congo red using MgO(111) nanoplates. The independence of Congo red adsorption from the pH suggests that, in addition to the electrostatic attraction, other adsorption mechanisms such as oxygen anions may also be involved.[38] Differences in the adsorption mechanisms of X3B and Congo red on MgO(111) nanoplates can be related to their physicochemical properties and structure. Similar results were reported for the adsorption of other reactive dyes from aqueous solutions.[34]

Effect of Temperature. Various textile dye effluents are produced at relatively high temperature; therefore, temperature can also be an important factor for the practical application of MgO(111). To determine whether the ongoing adsorption process was endothermic or exothermic in nature, Congo red and X3B of adsorption on MgO(111) were carried out at (283, 313, and 333) K at the initial dye concentration of 100 $mg \cdot L^{-1}$, MgO(111) dosage of 1.25 $g \cdot L^{-1}$, and contact time of 6 h. In general, the adsorption of Congo red increased with an increase of temperature as shown in Figure S4 of the SI, which indicates that the process was endothermic in both cases.

Effect of Ionic Strength. The ionic strength of the solution is one of the factors that control both electrostatic and nonelectrostatic interactions between the dye and the adsorbent surface. To determine whether the ongoing adsorption process was affected by salt (ionic strength), reactive dye adsorption studies over MgO(111) powders were carried out at sodium chloride concentrations of (0, 0.25, and 0.5) M with the constant initial dye concentration of 100 $mg \cdot L^{-1}$, adsorbent dosage of 0.015 g, and a stirring time of 30 min. The dye adsorption would be affected not only by the pH value on the electron-donating capability and temperature on the change of entropy and heat of reaction, but also by the salt concentration on the hydrophobic and electrostatic interaction between dye and surface functional adsorptive sites of the MgO(111). The adsorption capacities of MgO(111) for X3B were decreased with increasing NaCl concentration from (0 to 0.5) M (Figure S5, Supporting Information). The reduction of X3B removal might be due to Cl^- ions competing with the X3B molecules, leading to the reduction of X3B removal efficiency. On the basis of the trend shown in Figure S5, the adsorption capacities of MgO(111) for Congo red were not significantly affected with increasing NaCl concentration from (0 to 0.5) M. This indicates that Cl^- ions do not compete with sulfonate groups of the dye molecules for the adsorption sites of MgO(111). From this point of view, this result indicates that the MgO(111) can be used for removal of acidic reactive dyes from salt containing water.

Conclusion

MgO(111) nanosheets with polar (111) surfaces were used as adsorbents for the removal of two typical textile dyes, reactive brilliant red X-3B and Congo red from wastewater, and exhibited much more favorable adsorptive properties than magnesium oxide powder (CP-MgO) and activated carbon. The maximum adsorption capabilities of the two dyes on MgO(111) nanoplates reached (254.3 and 297.0) $mg \cdot g^{-1}$ for reactive brilliant red X-3B and Congo red, respectively. Isotherm modeling revealed that the Langmuir equation could better describe the adsorption of dyes on the MgO(111) as compared to other models. Kinetic data were appropriately fitted with the pseudosecond-order adsorption rates. MgO(111) demonstrated favorable adsorption behavior for both Congo red and X3B likely because of the high SSA, polar surface, and nanoscale particle size. The pH, ionic strength, and temperature played a significant role in affecting the dye adsorption capacity of the MgO(111) nanoplates. Differences in the adsorption mechanisms of X3B and Congo red on MgO(111) nanoplates can be related to their physicochemical properties and structure. MgO(111) is a nontoxic material and can be made in a simple and cost-effective way for the application and can be readily recycled and reused. These unique features present MgO (111) as a novel, promising, and feasible alternative for dye removal.

Supporting Information Available:

TEM images and local FFT of MgO nanosheets, tables of the adsorption parameter of isotherm and adsorption parameters of kinetics, and figures of the effect of the initial pH, temperature, and ionic strength on the removal of Congo red and X3B. This material is available free of charge via the Internet at http://pubs.acs.org.

Literature Cited

(1) Blackburn, R. S. Natural polysaccharides and their interactions with dye molecules: applications in effluent treatment. *Environ. Sci. Technol.* **2004**, *38*, 4905–4909.
(2) Gottlieb, A.; Shaw, C.; Smith, A.; Wheatley, A.; Forsythe, S. The toxicity of textile reactive azo dyes after hydrolysis and decolourisation. *J. Biotechnol.* **2003**, *101*, 49–56.
(3) Chahbane, N.; Popescu, D. L.; Mitchell, D. A.; Chanda, A.; Lenoir, D.; Ryabov, A. D.; Schramm, K. W.; Collins, T. J. Fe^{III}-TAML-catalyzed green oxidative degradation of the azo dye Orange II by H_2O_2 and organic peroxides: products, toxicity, kinetics, and mechanisms. *Green Chem.* **2007**, *9*, 49–57.

(4) Rai, H. S.; Bhattacharyya, M. S.; Singh, J.; Bansal, T. K.; Vats, P.; Banerjee, U. C. Removal of dyes from the effluent of textile and dyestaff manufacturing industry: A review of emerging techniques with reference to biological treatment. *Crit. Rev. Environ. Sci. Technol.* **2005**, *35*, 219–238.
(5) Valix, M.; Cheung, W. H.; McKay, G. Roles of the textural and surface chemical properties of activated carbon in the adsorption of acid blue dye. *Langmuir* **2006**, *22*, 4574–4582.
(6) Ko, D. C. K.; Tsang, D. H. K.; Porter, J. F.; McKay, G. Applications of multipore model for the mechanism identification during the adsorption of dye on activated carbon and bagasse pith. *Langmuir* **2003**, *19*, 722–730.
(7) Ho, K. Y.; McKay, G.; Yeung, K. L. Selective adsorbents from ordered mesoporous silica. *Langmuir* **2003**, *19*, 3019–3024.
(8) Liu, P.; Zhang, L. X. Adsorption of dyes from aqueous solutions or suspensions with clay nano-adsorbents. *Sep. Purif. Technol.* **2007**, *58*, 32–39.
(9) Ozdemir, Y.; Doqan, M.; Alkan, M. Adsorption of cationic dyes from aqueous solutions by sepiolite. *Microporous Mesoporous Mater.* **2006**, *96*, 419–427.
(10) Lazaridis, N. K.; Kyzas, G. Z.; Vassiliou, A. A.; Bikiaris, D. N. Chitosan derivatives as biosorbents for basic dyes. *Langmuir* **2007**, *23*, 7634–7643.
(11) Wong, Y. C.; Szeto, Y. S.; Cheung, W. H.; McKay, G. Equilibrium studies for acid dye adsorption onto chitosan. *Langmuir* **2003**, *19*, 7888–7894.
(12) Bekiari, V.; Lianos, P. Ureasil gels as a highly efficient adsorbent for water purification. *Chem. Mater.* **2006**, *18*, 4142–4146.
(13) Maffei, A. V.; Budd, P. M.; McKeown, N. B. Adsorption studies of a microporous phthalocyanine network polymer. *Langmuir* **2006**, *22*, 4225–4229.
(14) Silva, J. P.; Sousa, S.; Rodriques, J.; Antunes, H.; Porter, J. J.; Goncalves, I.; Ferreira-Dias, S. Adsorption of acid orange 7 dye in aqueous solutions by spent brewery grains. *Sep. Purif. Technol.* **2004**, *40*, 309–315.
(15) Mittal, A.; Krishnan, L.; Gupta, V. K. Removal and recovery of malachite green from wastewater using an agricultural waste material, de-oiled soya. *Sep. Purif. Technol.* **2005**, *43*, 125–133.
(16) Fugestu, B.; Satoh, S.; Shiba, T.; Mizutani, T.; Lin, Y. B.; Terui, N.; Nodasaka, Y.; Sasa, K.; Shimizu, K.; Akasaka, T.; Shindoh, M.; Shibata, K. I.; Yokoyama, A.; Mori, M.; Tanaka, K.; Sato, Y.; Tohji, K.; Tanaka, S.; Nishi, N.; Watari, F. Caged multiwalled carbon nanotubes as the adsorbents for affinity-based elimination of ionic dyes. *Environ. Sci. Technol.* **2004**, *38*, 6890–6896.
(17) Lee, C. K.; Lin, K. S.; Wu, C. F.; Lyu, M. D.; Lo, C. C. Effects of synthetic temperature on the microstructures and basic dyes adsorption of titanate nanotubes. *J. Hazard. Mater.* **2008**, *150*, 494–503.
(18) Chakrabarti, S.; Dutta, B. K. On the adsorption and diffusion of Methylene Blue in glass fibers. *J. Colloid Interface Sci.* **2005**, *286*, 807–811.
(19) Asok, A.; Bandyopadhyay, M.; Pal, A. Removal of crystal violet dye from wastewater by surfactant-modified alumina. *Sep. Purif. Technol.* **2005**, *44*, 139–144.
(20) Fei, J.; Cui, Y.; Yan, X.; Qi, W.; Yang, Y.; Wang, K.; He, Q.; Li, J. Controlled preparation of MnO_2 hierarchical hollow nanostructures and their application in water treatment. *Adv. Mater.* **2008**, *20*, 452–456.
(21) Zhong, L.; Hu, J.; Liang, H.; Cao, A.; Song, W.; Wan, L. Self-assembled 3D flowerlike iron oxide nanostructures and their application in water treatment. *Adv. Mater.* **2006**, *18*, 2426–2431.
(22) Salvador, F.; Sanchez Jimenez, C. A new method for regenerating activated carbon by thermal desorption with liquid water under subcritical conditions. *Carbon* **1996**, *34*, 511–516.
(23) Goto, M.; Hayashi, N.; Goto, S. Adsorption and desorption of phenol on anion-exchange resin and activated carbon. *Environ. Sci. Technol.* **1986**, *20*, 463–467.
(24) Narbaitz, R. M.; Cen, J. Electrochemical regeneration of granular activated carbon. *Water Res.* **1994**, *28*, 1771–1778.
(25) Hatchinson, D. H.; Robinson, C. W. A microbial regeneration process for granular activated carbon II. Regeneration studies. *Water Res.* **1990**, *24*, 1217–1223.
(26) Nagappa, B.; Chandrappa, G. T. Mesoporous nanocrystalline magnesium oxide for environmental remediation. *Microporous Mesoporous Mater.* **2007**, *106*, 212–218.
(27) Neppolian, B.; Wang, Q.; Jung, H.; Choi, H. Ultrasonic-assisted sol-gel method of preparation of TiO_2 nano-particles: characterization, properties and 4-chlorophenol removal application. *Ultrason. Sonochem.* **2008**, *15*, 649–658.
(28) Zelmanov, G.; Semiat, R. Iron(III) oxide-based nanoparticles as catalysts in advanced organic aqueous oxidation. *Water Res.* **2008**, *42*, 492–498.
(29) Hu, Z. G.; Zhang, J.; Chan, W. L.; Szeto, Y. S. The sorption of acid dye onto chitosan nanoparticles. *Polymer* **2006**, *47*, 5838–5842.
(30) Shu, H. Y.; Chang, M. C.; Yu, H.-H.; Chen, W. H. Removal of diazo dye Acid Black 24 in synthesized wastewater using zero-valent iron nanoparticle. *J. Colloid Interface Sci.* **2007**, *314*, 89–97.
(31) Mishakov, I. V.; Bedilo, A. F.; Richards, R. M.; Chesnokov, V. V.; Volodin, A. M.; Zaikovskii, V. I.; Buyanov, R. A.; Klabunde, K. J. Nanocrystalline MgO as a dehydrohalogenation catalyst. *J. Catal.* **2002**, *206*, 40–48.
(32) Richards, R.; Mulukutla, R. S.; Mishakov, I.; Chesnokov, V.; Volodin, A.; Zaikovski, V.; Sun, N.; Klabunde, K. J. Nanocrystalline ultra high surface area magnesium oxide as a selective base catalyst. *Scr. Mater.* **2001**, *44*, 1663–1666.
(33) Crittenden, J. C.; Trussell, R. R.; Hand, D. W.; Howe, K. J.; Tchobanoglous, G. *Water treatment: principals and design*, 2nd ed.; MWH, John Wiley and Sons, Inc.: New York, 2005.
(34) Gholamreza, M.; Maryam, M. Removal of azo and anthraquinone reactive dyes from industrial wastewaters using MgO nanoparticles. *J. Hazard. Mater.* **2009**, *168*, 806–812.
(35) Ranjit, K. T.; Klabunde, K. J. An aid in understanding the formation of porous inorganic materials. *Chem. Mater.* **2005**, *17*, 65–73.
(36) Diao, Y.; Walawander, W. P.; Sorensen, C. M.; Klabunde, K. J.; Thomas, R. Hydrolysis of magnesium methoxide. Effects of toluene on gel structure and gel chemistry. *Chem. Mater.* **2002**, *14*, 362–368.
(37) Li, W. C.; Lu, A. H.; Weidenthaler, C.; Schueth, F. Hard-templating pathway to create mesoporous magnesium oxide. *Chem. Mater.* **2004**, *16*, 5676–5681.
(38) Hu, J. C.; Zhu, K. K.; Chen, L. F.; Kuebel, C.; Richards, R. MgO(111) Nanosheets with unusual surface activity. *J. Phys. Chem.* **2007**, *111*, 12038–12044.
(39) Pengthamkeerati, P.; Satapanajaru, T.; Singchan, O. Sorption of reactive dye from aqueous solution on biomass fly ash. *J. Hazard. Mater.* **2008**, *153*, 1149–1156.
(40) Tan, I. A. W.; Ahmad, A. L.; Hameed, B. H. Equilibrium and kinetic studies of methyl violet sorption by agricultural waste. *J. Hazard. Mater.* **2008**, *154*, 337–346.
(41) Jain, R.; Sikarwar, S. Removal of hazardous dye congored from waste material. *J. Hazard. Mater.* **2008**, *152* (3), 942–948.
(42) Asim, O.; Necip, A. Equilibrium and kinetic adsorption study of Basic Yellow 28 and Basic Red 46 by a boron industry waste. *J. Hazard. Mater.* **2009**, *161*, 148–156.
(43) Freundlich, H. M. F. Ueber die adsorption in lösungen. *Z. Phys. Chem. (Leipzig)* **1906**, *57A*, 385–470.
(44) Oezcan, A. S.; Erdem, B. Adsorption of Acid Blue 193 from aqueous solutions onto BTMA-bentonite. *Colloids Surf., A* **2005**, *266*, 73–78.
(45) Langmuir, I. The constitution and fundamental properties of solids and liquids. Part I. solids. *J. Am. Chem. Soc.* **1916**, *38*, 2221–2295.
(46) Santos, S. C. R.; Vilar, V. J. P.; Boaventura, R. A. R. Waste metal hydroxide sludge as adsorbent for a reactive dye. *J. Hazard. Mater.* **2008**, *153*, 999–1008.
(47) Lagergren, S.; Kungliga, S. Zur theorie der sogenannten adsorption geloester stoffe. *Vetenskapsakad. Handlingar* **1898**, *24*, 1–39.
(48) Ho, Y. S.; McKay, G. Pseudo-second order model for sorption processes. *Process Biochem.* **1999**, *34*, 451–465.
(49) Acemioğlu, B. Adsorption of Congo red from aqueous solution onto calcium-rich fly ash. *J. Colloid Interface Sci.* **2004**, *274*, 371–379.
(50) Pavan, F.; Dias, S.; Lima, E.; Benvenutti, E. Removal of Congo red from aqueous solution by anilinepropylsilica xerogel. *Dyes Pigm.* **2008**, *76*, 64–69.
(51) Namasivayam, C.; Kavitha, D. Removal of Congo Red from water by adsorption onto activated carbon prepared from coir pith, an agricultural solid waste. *Dyes Pigm.* **2002**, *54*, 47–58.
(52) Al-Degs, Y. S.; El-Barghouthi, M. I.; El-Sheikh, A. H.; Walker, G. M. Effect of solution pH, ionic strength, and temperature on adsorption behavior of reactive dyes on activated carbon. *Dyes Pigm.* **2008**, *77*, 16–23.
(53) Wang, X.; Zhu, N.; Yin, B. Preparation of sludge-based activated carbon and its application in dye wastewater treatment. *J. Hazard. Mater.* **2008**, *153*, 22–27.

Received for review March 22, 2010. Accepted July 2, 2010. This work is supported by National Natural Science Foundation of China (20803096), the Scientific Research Foundation for the Returned Overseas Chinese Scholars, and State Education Ministry and South-Central University for Nationalities (YZZ 08002). L.C. thanks East China University of Science and Technology, the Fundamental Research Funds for Central Universities, Science and Technology Commission of Shanghai Municipality (10ZR1407200).

JE100274E